

Thermodynamics and efficiency of sequentially collisional Brownian particles: The role of drivings

Non Peer-reviewed author version

Fernando Filho, S.; Akasaki, Bruno A. N.; Noa, Carlos E. F.; CLEUREN, Bart & Fiore, Carlos E. (2022) Thermodynamics and efficiency of sequentially collisional Brownian particles: The role of drivings. In: PHYSICAL REVIEW E, 106 (4) (Art N° 044134).

DOI: 10.1103/PhysRevE.106.044134

Handle: <http://hdl.handle.net/1942/38905>

Thermodynamics and efficiency of sequentially collisional Brownian particles: The role of drivings

Fernando S. Filho,¹ Bruno A. N. Akasaki,¹ Carlos E. F. Noa,¹ Bart Cleuren,² and Carlos E. Fiore¹

¹Universidade de São Paulo, Instituto de Física, Rua do Matão, 1371, 05508-090 São Paulo, SP, Brasil

²UHasselt, Faculty of Sciences, Theory Lab, Agoralaan, 3590 Diepenbeek, Belgium

(Dated: June 14, 2022)

Brownian particles placed sequentially in contact with distinct thermal reservoirs and subjected to external driving forces are promising candidates for the construction of reliable thermal engines. In this contribution, we address the role of driving forces for enhancing the machine performance. Analytical expressions for thermodynamic quantities such as power output and efficiency are obtained for general driving schemes. A proper choice of these driving schemes substantially increases both power output and efficiency and extends the working regime. Maximizations of power and efficiency, whether with respect to the strength of the force, driving scheme or both have been considered and exemplified for two kind of drivings: a generic power-law and a periodically drivings.

I. INTRODUCTION

The construction of nanoscale engines has received a great deal of attention and recent technological advances have made feasible the realization of distinct setups such as quantum-dots [1], colloidal particles [2–4], single and coupled systems [5, 6] acting as working substance and others [7]. In contrast to their macroscopic counterparts, their main features are strongly influenced by fluctuations when operating at the nanoscale, having several features described within the framework of Stochastic Thermodynamics [8–12].

Recently a novel approach, coined collisional, has been put forward as a candidate for the projection of reliable thermal engines [13–17]. They consist of sequentially placing the system (a Brownian particle) in contact with distinct thermal reservoirs and subjected to external driving forces during each stage (stroke) of the cycle. Each stage is characterised by the temperature of the connected thermal reservoir and the external driving force. The time needed to switch between the thermal baths at the end of each stage is neglected. Despite its reliability in distinct situations, such as systems interacting only with a small fraction of the environment and those presenting distinct drivings over each member of system [18–21], the engine can operate rather inefficient depending on the way it is projected (temperatures, kind of driving and duration of each stroke). Hence the importance for strategies to enhance its performance [16, 17]. Among the distinct approaches, we cite those based on the maximization of power [10, 22–31], efficiency [16, 32, 33], low/finite dissipation [34, 35] or even the assumption of maximization via largest dissipation [36].

This paper deals with the above points but with a focus on a different direction, namely the optimization of the engine performance by fine-tuning the driving at each stroke. Such idea is illustrated in a collisional Brownian machine, which has been considered as a working substance in several works, as from the theoretical [6, 37–41] and experimental point of views [3, 33, 42–44]. The collisional description allows to derive general (and exact) expressions for thermodynamic quantities, such as output power and efficiency, irrespective of the kind of driving [16]. In order to exploit the consequences of a distinct driving each stroke and possible optimizations, two representative examples will be considered: periodically

and (generic) power-law drivings. The former consists of a simpler and feasible way to drive Brownian particles out of equilibrium [33, 43, 45–47] and providing simultaneous maximizations of the engine [6]. The latter has been considered not only for generalizing the machine performance beyond constant and linear drivings [15, 16], but also to exploit the possibility of obtaining a gain by changing its form at each stroke.

This paper is organized as follows: Sec. II presents the model and the main expressions for the thermodynamic quantities. Efficiency and optimisation is discussed in detail for both classes of drivings in Sec. III. Conclusions and perspectives are addressed in Sec. IV.

II. THERMODYNAMICS AND MAIN EXPRESSIONS

We focus on the simplest projection of an engine composed of only two strokes and returning to the initial step after one cycle. The time it takes to complete one cycle is set to τ , with each stroke $\in \{1, 2\}$ lasting a time $\tau/2$. During stroke i the Brownian particle of mass m is in contact with a thermal bath at temperature T_i and subjected to the external force $\tilde{f}_i(t)$.

In order to introduce thermodynamic forces and fluxes, we start from the expression for the steady entropy production (averaged over a complete period) given by $\bar{\sigma} = \bar{Q}_1/T_1 + \bar{Q}_2/T_2$, where \bar{Q}_1 and \bar{Q}_2 are the exchanged heat in each stroke. By resorting to the first law of Thermodynamics $\bar{Q}_1 + \bar{Q}_2 = -(\bar{W}_1 + \bar{W}_2)$ and expressing T_1 and T_2 in terms of the mean T and the difference $\Delta T = T_2 - T_1$, $\bar{\sigma}$ can be rewritten in the following (general) form:

$$\bar{\sigma} = \frac{4T^2}{4T^2 - \Delta T^2} \left[-\frac{1}{T} (\bar{W}_1 + \bar{W}_2) + (\bar{Q}_1 - \bar{Q}_2) \frac{\Delta T}{2T^2} \right]. \quad (1)$$

Expressions for work and heat are obtained by considering the time evolution of the system probability distribution $P_i(v, t)$, governed by the following Fokker-Planck (FP) equation [11, 48, 49]

$$\frac{\partial P_i}{\partial t} = -\frac{\partial J_i}{\partial v} - \tilde{f}_i(t) \frac{\partial P_i}{\partial v}. \quad (2)$$

Here J_i denotes the probability current given by

$$J_i = -\gamma_i v P_i - \frac{\gamma_i k_B T_i}{m} \frac{\partial P_i}{\partial v}, \quad (3)$$

with γ_i the viscous coefficient per mass. Applying the usual boundary conditions in the space of velocities, in which both $P_i(v, t)$ and $J_i(v, t)$ vanish as $|v| \rightarrow \infty$, the time evolution of system energy $U_i(t) = m\langle v_i^2 \rangle / 2$ during each stroke corresponds to the sum of two terms:

$$\frac{d}{dt} U_i(t) = -[\dot{W}_i(t) + \dot{Q}_i(t)] \quad (4)$$

with the mean power $\dot{W}_i(t)$ and heat $\dot{Q}_i(t)$ given by

$$\dot{W}_i(t) = -m\langle v_i \rangle(t) \tilde{f}_i(t); \quad (5)$$

$$\dot{Q}_i(t) = \gamma_i \left(m \langle v_i^2 \rangle(t) - k_B T_i \right). \quad (6)$$

By averaging over a complete period, one recovers the first law of Thermodynamics as stated previously. Similarly, the time evolution of the system entropy $S_i(t) = -k_B \langle \ln P_i \rangle$ during stage i can be expressed as a difference between two terms:

$$\frac{d}{dt} S_i = \sigma_i(t) - \Phi_i(t), \quad (7)$$

where $\sigma_i(t)$ and $\Phi_i(t)$ are the entropy production rate and the entropy flux, respectively, whose expressions are given by

$$\sigma_i(t) = \frac{m}{\gamma_i T_i} \int \frac{J_i^2}{P_i} dv, \quad \text{and} \quad \Phi_i(t) = \frac{\dot{Q}_i(t)}{T_i}. \quad (8)$$

Note that the right side of Eq. (8) integrated over a complete period is equivalent with the relation for $\bar{\sigma}$ given by Eq. (1). Expressions for above thermodynamic quantities in terms of system parameters are obtained by recalling that such class of systems evolve to a nonequilibrium steady state whose probability distribution $P_i(v, t)$ for the i -th stage, satisfying Eq. (2), is Gaussian,

$$P_i(v, t) = \exp\left\{-\frac{(v - \langle v_i \rangle(t))^2}{2b_i(t)}\right\} / \sqrt{2\pi b_i(t)} \quad (9)$$

in which the mean $\langle v_i \rangle(t)$ and variance $b_i(t) = \langle v_i^2 \rangle(t) - \langle v_i \rangle^2(t)$ are time dependent and determined by the following equations

$$\frac{d\langle v_i \rangle(t)}{dt} = -\gamma_i \langle v_i \rangle(t) + \tilde{f}_i(t), \quad (10)$$

and

$$\frac{db_i(t)}{dt} = -2\gamma_i b_i(t) + \frac{2\gamma_i k_B T_i}{m}, \quad (11)$$

respectively. In order to obtain explicit and general results, external forces are expressed in the following form:

$$\tilde{f}_i(t) = \begin{cases} X_1 g_1(t), & t \in [0, \tau/2] \\ X_2 g_2(t), & t \in [\tau/2, \tau], \end{cases} \quad (12)$$

where $g_i(t)$ and X_i account for the kind of driving and its strength at stage i , respectively. Continuity of $P_i(v, t)$ at times $t = \tau/2$ and $t = \tau$ implies

$$\langle v_1 \rangle(\tau/2) = \langle v_2 \rangle(\tau/2) \quad ; \quad b_1(\tau/2) = b_2(\tau/2) \quad (13)$$

$$\langle v_1 \rangle(0) = \langle v_2 \rangle(\tau) \quad ; \quad b_1(0) = b_2(\tau) \quad (14)$$

From the above, we arrive at the following general expressions (evaluated for $k_B = 1$ and equal $\gamma_i = \gamma$):

$$\langle v_1 \rangle(t) = X_1 \int_0^t e^{\gamma(t-t')} g_1(t') dt' + \frac{1}{e^{\gamma t} - 1} \left\{ X_1 \int_0^{\tau/2} e^{\gamma(t-t')} g_1(t') dt' + X_2 \int_{\tau/2}^{\tau} e^{\gamma(t-t')} g_2(t') dt' \right\}, \quad (15)$$

$$\langle v_2 \rangle(t) = X_2 \int_{\tau/2}^t e^{\gamma(t-t')} g_2(t') dt' + \frac{1}{e^{\gamma t} - 1} \left\{ e^{\gamma t} X_1 \int_0^{\tau/2} e^{\gamma(t-t')} g_1(t') dt' + X_2 \int_{\tau/2}^{\tau} e^{\gamma(t-t')} g_2(t') dt' \right\}, \quad (16)$$

$$b_1(t) = -\frac{1}{m} \frac{(T_1 - T_2)}{(1 + e^{-\gamma t})} e^{-2\gamma t} + \frac{T_1}{m} \quad ; \quad b_2(t) = -\frac{1}{m} \frac{(T_2 - T_1)}{(1 + e^{-\gamma t})} e^{-2\gamma(t-\tau/2)} + \frac{T_2}{m}. \quad (17)$$

Inserting the above expressions into Eqs. (5-6) and averaging over a complete cycle we finally arrive at

$$\begin{aligned} \bar{W}_1 = & -\frac{m}{\tau(e^{\gamma\tau} - 1)} \left[X_1^2 \left((e^{\gamma\tau} - 1) \int_0^{\tau/2} g_1(t) e^{-\gamma t} \int_0^t g_1(t') e^{\gamma t'} dt' dt + \int_0^{\tau/2} g_1(t) e^{-\gamma t} dt \int_0^{\tau/2} g_1(t') e^{\gamma t'} dt' \right) \right. \\ & \left. + X_1 X_2 \int_0^{\tau/2} g_1(t) e^{-\gamma t} dt \int_{\tau/2}^{\tau} g_2(t') e^{\gamma t'} dt' \right], \end{aligned} \quad (18)$$

$$\bar{Q}_1 = \frac{\gamma m}{\tau} \left[\int_0^{\tau/2} \langle v_1 \rangle^2 dt - \frac{1}{2\gamma m} \tanh(\gamma\tau/2) (T_1 - T_2) \right], \quad (19)$$

and

$$\begin{aligned} \bar{W}_2 = & -\frac{m}{\tau(e^{\gamma\tau} - 1)} \left[X_2^2 \left(\int_{\tau/2}^{\tau} g_2(t)e^{-\gamma t} dt \int_{\tau/2}^{\tau} g_2(t')e^{\gamma t'} dt' + (e^{\gamma\tau} - 1) \int_{\tau/2}^{\tau} g_2(t)e^{-\gamma t} \int_{\tau/2}^t g_2(t')e^{\gamma t'} dt' dt \right) \right. \\ & \left. + X_1 X_2 \left(\int_{\tau/2}^{\tau} g_2(t)e^{-\gamma t} dt \int_0^{\tau/2} g_1(t')e^{\gamma t'} dt' + (e^{\gamma\tau} - 1) \int_{\tau/2}^{\tau} e^{-\gamma t} g_2(t) dt \int_0^{\tau/2} e^{\gamma t'} g_1(t) dt' \right) \right], \end{aligned} \quad (20)$$

$$\bar{Q}_2 = \frac{m\gamma}{\tau} \left[\int_{\tau/2}^{\tau} \langle v_2 \rangle^2 dt + \frac{1}{2\gamma m} \tanh(\gamma\tau/2)(T_1 - T_2) \right], \quad (21)$$

for first and second stages, respectively and $\bar{\sigma}$ is promptly obtained by inserting above expressions in Eq. (1). It is worth emphasizing that Eqs. (18)-(21) are general and valid for any kind of drivings and temperatures. Close to equilibrium the entropy production (Eq. (1)) assumes the familiar *flux times force* form $\bar{\sigma} \approx J_1 f_1 + J_2 f_2 + J_T f_T$ with forces

$$f_1 = X_1/T ; f_2 = X_2/T ; f_T = \Delta T/T^2 \quad (22)$$

($\Delta T = T_2 - T_1$) and fluxes defined by

$$\bar{W}_1 = -T J_1 f_1 ; \bar{W}_2 = -T J_2 f_2 ; \bar{Q}_1 - \bar{Q}_2 = 2 J_T. \quad (23)$$

Up to first order in the forces these fluxes can be expressed in terms of Onsager coefficients $J_1 = L_{11} f_1 + L_{12} f_2$, $J_2 = L_{21} f_1 + L_{22} f_2$ and $J_T = L_{TT} f_T$ which results in

$$L_{11} = \frac{mT}{\tau(e^{\gamma\tau} - 1)} \left[(e^{\gamma\tau} - 1) \int_0^{\tau/2} g_1(t)e^{-\gamma t} \int_0^t g_1(t')e^{\gamma t'} dt' dt + \int_0^{\tau/2} g_1(t)e^{-\gamma t} dt \int_0^{\tau/2} g_1(t')e^{\gamma t'} dt' \right], \quad (24)$$

$$L_{22} = \frac{mT}{\tau(e^{\gamma\tau} - 1)} \left[\int_{\tau/2}^{\tau} g_2(t)e^{-\gamma t} dt \int_{\tau/2}^{\tau} g_2(t')e^{\gamma t'} dt' + (e^{\gamma\tau} - 1) \int_{\tau/2}^{\tau} g_2(t)e^{-\gamma t} \int_{\tau/2}^t g_2(t')e^{\gamma t'} dt' dt \right], \quad (25)$$

$$L_{12} = \frac{mT}{\tau(e^{\gamma\tau} - 1)} \int_0^{\tau/2} g_1(t)e^{-\gamma t} dt \int_{\tau/2}^{\tau} g_2(t')e^{\gamma t'} dt' ; \quad L_{21} = \frac{mT e^{\gamma\tau}}{\tau(e^{\gamma\tau} - 1)} \int_0^{\tau/2} g_1(t')e^{\gamma t'} dt' \int_{\tau/2}^{\tau} g_2(t)e^{-\gamma t} dt, \quad (26)$$

$$L_{TT} = \frac{T^2}{2\tau} \tanh\left(\frac{\gamma\tau}{2}\right). \quad (27)$$

Two remarks are in order. First, to verify Onsager-Casimir symmetry for the cross coefficients L_{12} and L_{21} it is necessary not only to reverse the drivings but also to exchange the indices $1 \leftrightarrow 2$ as argued in [14]. Second, there is no coupling between work fluxes and heat flux. That is, the cross coefficients L_{T1} , L_{1T} , L_{T2} and L_{2T} are absent. Hence this class of engines does not convert heat into work (and vice versa) and always loses its efficiency when the difference of temperatures ΔT between thermal baths is large, because heat can not be converted into output work [6, 16].

As we gonna see next, for the regime of temperatures we shall concern, efficiency properties can be solely expressed in terms of Onsager coefficients and their derivatives.

III. EFFICIENCY

As stated before, our aim is to adjust the drivings in order to optimize the system performance. More concretely, given an amount of energy \bar{W}_{in} injected to the system, whether in the form of input work $\bar{W}_{in} \equiv \bar{W}_1 < 0$ and/or heat $\bar{Q}_{in} = \bar{Q}_1 \Theta(-\bar{Q}_1) + \bar{Q}_2 \Theta(-\bar{Q}_2) < 0$ ($\Theta(x)$ denoting the Heaviside function), it is partially converted into power output $\mathcal{P} \equiv \bar{W}_2 \geq 0$. A measure

of such conversion is characterized by the efficiency, given as the ratio between above quantities:

$$\eta = -\frac{\mathcal{P}}{\bar{W}_{in} + \bar{Q}_{in}}. \quad (28)$$

In order to obtain a first insight about the role driving, we shall split the analysis in two parts: engine operating at an unique temperature but the driving is changed each half stage. Next, we extend for different temperatures and distinct drivings.

A. Overview about Brownian work-to-work converters and distinct maximizations routes

Work-to-work converters have been studied broadly in the context of biological motors such as kinesin [50, 51] and myosin, in which chemical energy is converted into mechanical and vice-versa [52]. More recently, distinct work-to-work converters made of Brownian engines have been attracted considerable attention and in this section we briefly revise their main aspects [6, 15, 16, 33, 53]. Setting $\Delta T = 0$ (hence $f_T = 0$) reduces the efficiency Eq. (28) to the ratio between

Onsager coefficients: [6, 15, 16]

$$\eta \equiv -\frac{\mathcal{P}}{\dot{W}_{\text{in}}} = -\frac{L_{22}f_2^2 + L_{21}f_1f_2}{L_{12}f_1f_2 + L_{11}f_1^2}. \quad (29)$$

For any kind of driving and period, the engine regime $\mathcal{P} > 0$ implies that the absolute value for the output force f_2 must lie in the interval $0 \leq |f_2| \leq |f_m|$, where $f_m = -L_{21}f_1/L_{22}$. Since power, efficiency and dissipation are not independent from each other, f_m can be related with f_{2mS} (for f_1 and driving parameter constants), in which the dissipation is minimal. It is straightforward to show that $f_m = f_{2mS} + (L_{12} - L_{21})f_1/(2L_{22})$. Note that $f_m = f_{2mS}$ only when the Onsager coefficients are symmetric, $L_{12} = L_{21}$.

Optimized quantities, whether power and efficiency, can be obtained under three distinct routes: optimization with respect to (i) the output force f_2 (keeping f_1 and a driving parameter δ fixed), (ii) the driving parameter δ (forces f_1 and f_2 held fixed) and (iii) a simultaneous optimization with respect to both f_2 and δ . As discussed in Refs. [15, 16, 33], such optimized quantities can be expressed in terms of Onsager coefficients and their derivatives.

The former case (maximization with respect to the output force) is similar to findings from Refs. [15, 16, 33], in which the maximum power \mathcal{P}_{MP,f_2} (with efficiency η_{MP,f_2}) and maximum efficiency η_{ME,f_2} (with power \mathcal{P}_{ME,f_2}) are obtained via optimal adjustments f_{2MP} and f_{2ME} . By taking the derivative of \mathcal{P} and Eq. (29) with respect to f_2 , f_{2ME} and f_{2MP} are given by

$$f_{2ME} = \frac{L_{11}}{L_{12}} \left(-1 + \sqrt{1 - \frac{L_{12}L_{21}}{L_{11}L_{22}}} \right) f_1 \quad \text{and} \quad f_{2MP} = -\frac{1}{2} \frac{L_{21}}{L_{22}} f_1, \quad (30)$$

and their associate efficiencies read

$$\eta_{ME,f_2} = -\frac{L_{21}}{L_{12}} + \frac{2L_{11}L_{22}}{L_{12}^2} \left(1 - \sqrt{1 - \frac{L_{12}L_{21}}{L_{11}L_{22}}} \right), \quad (31)$$

and

$$\eta_{MP,f_2} = \frac{L_{21}^2}{4L_{11}L_{22} - 2L_{12}L_{21}}, \quad (32)$$

respectively. Analogous expressions for the power at maximum efficiency \mathcal{P}_{ME,f_2} and the maximum power \mathcal{P}_{MP,f_2} can be obtained by inserting f_{2ME} or f_{2MP} into the expression for \mathcal{P} . As stated before, the second maximization to be considered is carried out for fixed output forces and a given driving parameter δ is adjusted ensuring maximum power δ_{MP} and/or efficiency δ_{ME} , respectively. According to Ref. [6, 16], they fulfill the following expressions

$$\frac{L'_{21}(\delta_{MP})}{L'_{22}(\delta_{MP})} = -\frac{f_2}{f_1}, \quad (33)$$

and

$$\Delta_{2212}(\delta_{ME})f_2^2 + \Delta_{2111}(\delta_{ME})f_1^2 + [\Delta_{2211}(\delta_{ME}) + \Delta_{2112}(\delta_{ME})]f_1f_2 = 0, \quad (34)$$

respectively, where $L'_{ij}(\delta) \equiv \partial L_{ij}(\delta)/\partial \delta$ is the derivative of coefficient L_{ij} respect to the driving δ and $\Delta_{ijkl}(\delta) = L'_{ij}(\delta)L_{kl}(\delta) - L'_{kl}(\delta)L_{ij}(\delta)$. Associate maximum power and efficiency are given by

$$\mathcal{P}_{MP,\delta} = \frac{L'_{21}(\delta_{MP})}{L_{22}^2(\delta_{MP})} [L_{21}(\delta_{MP})L'_{22}(\delta_{MP}) - L_{22}(\delta_{MP})L'_{21}(\delta_{MP})] f_1^2, \quad (35)$$

and

$$\eta_{ME,\delta} = -\frac{L_{22}(\delta_{ME})f_2^2 + L_{21}(\delta_{ME})f_1f_2}{L_{11}(\delta_{ME})f_1^2 + L_{12}(\delta_{ME})f_1f_2}, \quad (36)$$

respectively, and expressions for $\mathcal{P}_{ME,\delta}$ and $\eta_{MP,\delta}$ are obtained under a similar way. Although exact and valid for any choice of the drivings $g_i(t)$ and forces f_i , Eqs. (33) and (34), in general, have to be solved numerically for achieving δ_{MP} and δ_{ME} .

In certain cases (as shall be explained next), it is possible to maximize the engine with respect to the output force f_2 and a driving parameter δ simultaneously, which corresponds to the crossing point between maximum lines (power or efficiency) with respect to f_2 and δ . More specifically, given the locus of maxima f_{2MP}/f_{2ME} (δ fixed) and δ_{MP}/δ_{ME} (f_2 fixed), the global $\delta_{MP}^*/\delta_{ME}^*$ and f_{2MP}^*/f_{2ME}^* corresponds to their intersection. For instance, the global maximization of power is given by Eqs. (30) and (33):

$$\frac{L'_{21}(\delta_{MP}^*)}{L'_{22}(\delta_{MP}^*)} = \frac{1}{2} \frac{L_{21}(\delta_{MP}^*)}{L_{22}(\delta_{MP}^*)} \quad \text{and} \quad f_{2MP}^* = -\frac{1}{2} \frac{L_{21}(\delta_{MP}^*)}{L_{22}(\delta_{MP}^*)} f_1, \quad (37)$$

whose (associate global) maximum power \mathcal{P}^* and efficiency η^* read

$$\mathcal{P}^* = \frac{1}{4} \frac{L_{21}^2(\delta_{MP}^*)}{L_{22}(\delta_{MP}^*)} f_1^2, \quad (38)$$

and

$$\eta^* = \frac{L_{21}^2(\delta_{MP}^*)}{4L_{11}(\delta_{MP}^*)L_{22}(\delta_{MP}^*) - 2L_{21}(\delta_{MP}^*)L_{12}(\delta_{MP}^*)}, \quad (39)$$

respectively.

B. Applications

Once introduced the main expressions, we are now in position for analyzing the role of driving in our two stage engine. For instance, we shall consider two distinct (but exhibiting complementary features) cases: generically periodically drivings and power-law drivings. As stated before, periodically drivings provided simultaneous maximizations of an autonomous engine [6]. In this contribution, we address a simultaneous maximization for our collisional engine. Conversely, power-law drivings has been considered in order to generalize the machine performance beyond constant and linear drivings as well as by exploiting the possibility of improving the engine performance via distinct drivings at each stage [15, 16].

1. Generic periodically driving forces

In this section, we apply the sequential engine under a general periodically driving, having its form and strength in each half stage expressed in terms of its Fourier components:

$$g_i(t) = \sum_{n=0}^{\infty} \left[a_n^{(i)} \cos\left(\frac{4\pi n}{\tau}t\right) + b_n^{(i)} \sin\left(\frac{4\pi n}{\tau}t\right) \right], \quad (40)$$

for the i -th stage ($i = 1$ or 2), where coefficients $a_0^{(i)}$, $a_n^{(i)}$ and $b_n^{(i)}$ are given by

$$a_0^{(i)} = \frac{2}{\tau} \int_{(i-1)\tau/2}^{i\tau/2} g_i(t') dt', \quad (41)$$

$$a_n^{(i)} = \frac{4}{\tau} \int_{(i-1)\tau/2}^{i\tau/2} g_i(t') \cos\left(\frac{4\pi n}{\tau}t'\right) dt', \quad (42)$$

$$b_n^{(i)} = \frac{4}{\tau} \int_{(i-1)\tau/2}^{i\tau/2} g_i(t') \sin\left(\frac{4\pi n}{\tau}t'\right) dt'. \quad (43)$$

Thermodynamic quantities and maximizations are also exactly obtained from Onsager coefficients, depending on Fourier coefficients $a_0^{(i)}$'s, $a_n^{(i)}$'s and $b_n^{(i)}$'s, whose expressions for generic periodically drivings are listed in Appendix A. In order to tackle the role of the driving under a simpler strategy, from now on, we shall restrict ourselves to the simplest case in which drivings at each stroke present the same frequency, but they differ from phase difference ϕ given by

$$g_1(t) = \sin\left(\frac{4\pi}{\tau}t\right) \quad ; \quad g_2(t) = \sin\left(\frac{4\pi}{\tau}t - \phi\right), \quad (44)$$

The inclusion of a lag ϕ in the second half stage has been inspired in recent works in which it can control of power, efficiency [6] and dissipation [54] and also by guiding the operation modes of the engine [6]. Fig. 1 depicts some features for distinct Tf_2 's and ϕ 's, respectively. First of all, the regime operation is delimited between 0 and $|f_{2m}|$ in which maximization obeys Eqs. (30) (acquiring simpler form given by Eq. [(45)]) and a similar expression (although cumbersome) is obtained for f_{2ME}/f_1 . Note that for $\gamma\tau \ll 1$ and $\gamma\tau \gg 1$, $f_{2MP}/f_1 \rightarrow 1/(2\cos\phi)$ and 0, respectively, such latter being independent on the lag, respectively.

$$\frac{f_{2MP}}{f_1} = \frac{4\pi \left(e^{\frac{\gamma\tau}{2}} + 1 \right) (2\pi \cos(\phi) - \gamma\tau \sin(\phi))}{\gamma\tau \left(\left(e^{\frac{\gamma\tau}{2}} - 1 \right) (\gamma^2\tau^2 + 4\pi^2) - 4\gamma\tau \left(e^{\frac{\gamma\tau}{2}} + 1 \right) \sin^2(\phi) \right) + 16\pi^2 \left(e^{\frac{\gamma\tau}{2}} + 1 \right) \cos^2(\phi)}, \quad (45)$$

Fig. 2 reveals additional (and new) features coming from the lag in the second stage. The former is the existence of a two distinct engine regimes for the some values of Tf_2 , being delimited between two intervals $\phi_{1m} \leq \phi \leq \phi_{2m}$ and $\phi_{3m} \leq \phi \leq \phi_{4m}$ (fulfilling $\mathcal{P} = 0$ at $\phi = \phi_{im}$). Also, the change of lag moves the engine regime from positive to negative of f_2 's. For example, for $\tau = 2$ the engine regime yields for positive (negative) output forces for $-\pi/2 < \phi \leq \pi/2$ ($\pi/2 < \phi \leq \pi$). Finally, in similarity with coupled harmonic chains [6], the lag also controls the engine performance, having optimal ϕ_{ME} and ϕ_{MP} in which $\eta_{ME,\phi}$ and $\mathcal{P}_{MP,\phi}$, respectively. They obey Eqs. (33)/(46) and (34), the former acquire a simpler expression

$$\frac{f_2}{f_1} = \frac{\pi[\gamma\tau \csc(\phi_{MP}) + 2\pi \sec(\phi_{MP})]}{\gamma^2\tau^2 + 4\pi^2}, \quad (46)$$

for the power and a more cumbersome (not shown) for ϕ_{ME} . In the limit of $\gamma\tau \ll 1$ and $\gamma\tau \gg 1$, Eq. (46) approaches to $\phi_{MP} \rightarrow \cos^{-1}(f_1/2f_2)$ and zero, respectively, such latter independent on the ratio between forces, respectively. For completeness, Fig. 3 extends aforementioned efficiency and power findings for other values of Tf_2 and ϕ . Note that suitable choices of ϕ and f_2 may lead to a substantial increase of engine performance. For example, for $\phi = 0$, the maximum $\mathcal{P}_{MP,\delta=0} \approx 0.0231$ and $\eta_{ME,\delta=0} \approx 0.494$, whereas a simultaneous maximization leads to a substantial increase of power-output [given by the intersection between Eqs. (45) and (46)]

$P^* \approx 0.0398$ and also of $\eta^* \approx 0.581$.

2. Power Law drivings

We consider a general algebraic (power-law) driving acting at each half stage:

$$g(t) = \begin{cases} \left(\frac{2t}{\tau}\right)^\alpha, & \text{for } t \in [0, \tau/2] \\ \left(1 - \frac{2t}{\tau}\right)^\beta, & \text{for } t \in [\tau/2, \tau], \end{cases} \quad (47)$$

where α and β assume non-negative values. It is worth mentioning that particular cases $\alpha = \beta = 0$ and $\alpha = \beta = 1$ were considered in Ref. [15]. In order to exploit in more details the influence of algebraic drivings into the first (being the worksource and heatsource) and second (responsible for the output work \mathcal{P}) stages, analysis will be carried out by changing each one of them separately [by keeping fixed β and α in the former and latter stages, respectively]. Although quantities can be straightforwardly obtained from Eqs. (18)-(26), expressions are very cumbersome (see e.g. appendix B) and for this reason analysis will be restricted for remarkable values of α and β . In principle, they can assume integer and half-integer values. Nonetheless, inspection of exact expressions reveal that Onsager coefficients assume imaginary values when β is half integer. Since half integer values α do not promote substantial changes (not shown), all analysis will be carried out for both

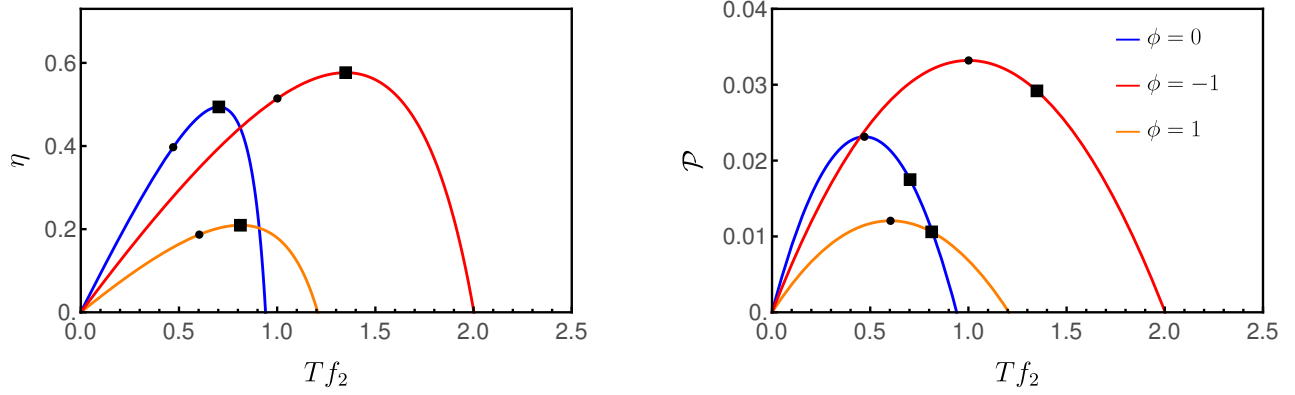


FIG. 1. For periodic drivings, the depiction of efficiency η and power-output \mathcal{P} versus force Tf_2 for distinct ϕ 's. Squares and circles denote the maximum efficiencies and powers, according to Eq. (31)-(30). In all cases, we set $X_1 = Tf_1 = 1$, $\tau = 2$, $\gamma = k_B = m = 1$ and $T = 1/2$.

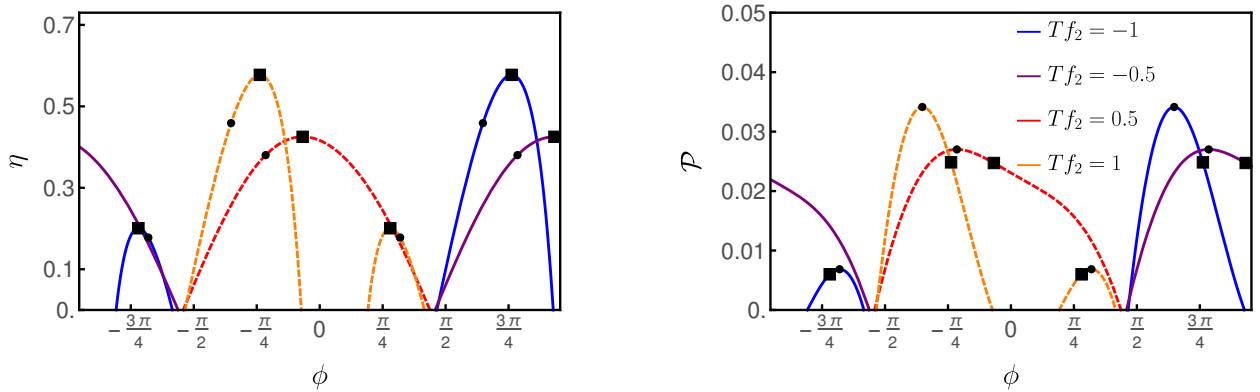


FIG. 2. For $\tau = 2$ and distinct Tf_2 's, depiction of efficiency η and power-output \mathcal{P} versus ϕ . Squares and circles denote the maximum efficiencies and powers, respectively, according to Eqs. (33) and (34). In all cases, we set $X_1 = Tf_1 = 1$, $\gamma = k_B = m = 1$ and $T = 1/2$.

α and β integers. Thermodynamics quantities are directly obtained from Eqs. (26), whose Onsager coefficients are listed in Appendix B.

Fig. 4 depicts the main portraits of the engine performance by varying the output force for some representative values of Tf_2 , α and β . Firstly, it reveals that the power output \mathcal{P} (left panels) is strongly (smoothly) dependent on the shape of driving acting over the first (second) half stage. In the former case, \mathcal{P} is larger for smaller α [having its maximum for time independent ones ($\alpha = \beta = 0$)] and always decreases (for all values of Tf_2) as α goes up. Unlike the substantial reduction of power output as α is raised, it is f_2 -dependent as β (for fixed α) is increased, in which \mathcal{P}_{mP,f_2} is mildly decreasing in such case. The increase of β confers some remarkable features, such as the substantial increase of range of output forces (e.g. $|f_{2m}|$ increases) in which the system operates as an engine, being restricted to positive (negative) f_2 's for odd (even) values of β . Complementary findings are achieved by examining the influence of drivings for the efficiency. Unlike the \mathcal{P} , η is f_2 -dependent but η_{mE,f_2} always increases as α is raised and mildly decreases as β goes up. Finally, we stress

that η_{mE,f_2} (squares) and η_{mP,f_2} (circles) in right panels obey Eqs. (31) and (32), respectively, having their associate \mathcal{P}_{mE,f_2} and \mathcal{P}_{mP,f_2} illustrated in the left panels.

Next, we tackle the opposite route, in which f_2 is kept fixed with α or β being varied in order to ensure optimal performance. Maximization of quantities follow theoretical predictions from Eqs. (33) and (34) and Fig. 5 depicts main trends for some representative values of f_2 .

The dependence of driving α upon the efficiency shares some similarities when compared with f_2 (panel (a)), leading to the existence of an optimal driving $\alpha > 0$ ($\alpha = 0$) for low (large) values of $|f_2|$. Hence, a driving beyond the constant case in the first stage can be important for increasing efficiency, depending on the way the machine is projected. On the other hand, for power-output purposes, $\mathcal{P}_{mP,\alpha=0}$'s are always maxima and decreases for $\alpha > 0$, irrespective to the value of output force (panel (c)).

The opposite case (fixed α and β is varied) is also more revealing and it is f_2 dependent (see e.g. panels (c)–(d) and Fig. 6), in which maximum efficiencies $\eta_{mE,\beta}$ and powers $\mathcal{P}_{mP,\beta}$ also follow Eqs. (34) and (33). Fig. 6 extends aforementioned

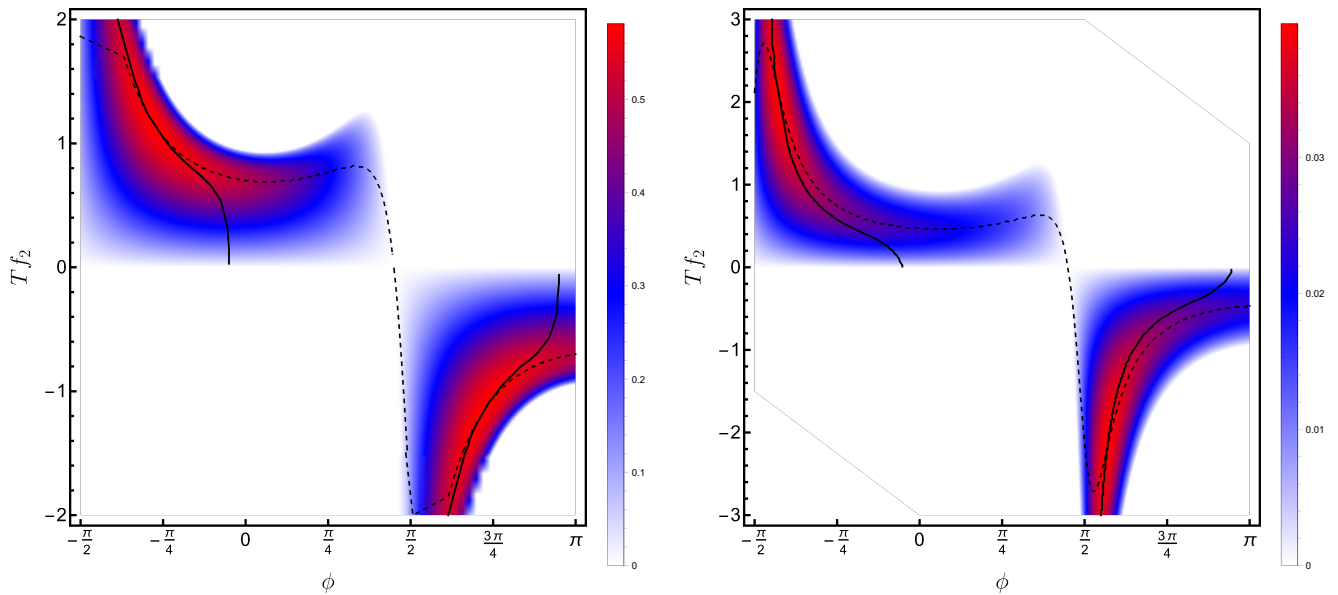


FIG. 3. For the set of drivings given by Eq. (44) and $\tau = 2$, left and right panels depict the phase diagram of the output force $X_2 = T f_2$ versus the phase difference ϕ for the efficiency and power output, respectively. Continuous and dashed lines denote the maximization with respect to f_2 and ϕ , respectively. In all cases, we set $X_1 = T f_1 = 1$, $\gamma = k_B = m = 1$ and $T = 1/2$.

findings for several values of α and β . In contrast the periodically drivings, a global optimization in such case has not been performed, since α and β present only integer values.

Summarizing above findings: While low α 's stage is always more advantageous for enhancing the power output, there is a compromise between force $|f_2|$ and α and β in order to en-

hance the efficiency. On the other hand, although maximum efficiencies and powers smoothly decreases with β , the set of output forces $|f_2|$ in which the system operates as an engine enlarges substantially.

C. Difference of temperatures

In this section we examine the effect of different drivings each stroke when the temperatures are also different. Since \mathcal{P} does not depend on the temperature, the numerator of Eq. (28) is the same as before, but now the system can receive heat from the thermal bath 1 or 2 if $T_1 > T_2$ or $T_1 < T_2$, respectively and hence such kind of engine becomes less efficiently when the difference of temperatures raises. We wish to investigate the interplay between parameters as a strategy for compensating above point. Taking into account that \bar{Q}_1 (or \bar{Q}_2) also depends on the f_1 and f_2 [appearing inside $\langle v_1 \rangle(t)$ (or $\langle v_2 \rangle(t)\Delta T$ the system will receive heat from a thermal bath 1 (2) only if $2m\gamma \int_0^{\tau/2} \langle v_1 \rangle^2 dt < \tanh(\gamma\tau/2)(T_1 - T_2)$ [$2m\gamma \int_{\tau/2}^{\tau} \langle v_2 \rangle^2 dt < \tanh(\gamma\tau/2)(T_2 - T_1)$]. Otherwise, the thermal engine will behave as a work-to-work converter and all previous analysis and expressions can be applied. For large ΔT (not considered here), above inequalities are always fulfilled and hence the system efficiency is always lower than the work-to-work case.

Figs. 7 and 8 exemplify thermal engines for periodically drivings. As stated before, although the system operates in a

similar way to the work-to-work converter for some values of $T f_2$ (see e.g. symbols \times separating the thermal from work-to-work regimes), the efficiency decreases as ΔT is raised, illustrating the no conversion of heat into output work. Interestingly, the system placed in contact with the hot thermal bath in the first stage leads to somewhat higher efficiencies ($\eta^* \approx 0.547$) than in the first stage $\eta^* \approx 0.433$). This can be understood by examining the first term in the right sides of Eqs. (19) and (21). Since the contribution coming from the difference of temperatures is the same in both cases, the interplay between lag and driving forces leads to $\int_0^{\tau/2} \langle v_1 \rangle^2(t) dt$ be larger than $\int_{\tau/2}^{\tau} \langle v_2 \rangle^2(t) dt$ and hence conferring some advantage when $T_1 > T_2$.

Lastly, Fig. 9 extends the results for thermal engines for power-law drivings. For all values of α and β , the thermal engine is marked by a reduction of its performance as $\Delta T \neq 0$, being more substantial as α is raised and less sensitive to the increase of driving in the second state (increase of β). Lastly, the engine performances also exhibit some (small) differences when the hot bath acts over the first and second strokes (see e.g. left and right panels), being somewhat larger when $\Delta T > 0$.

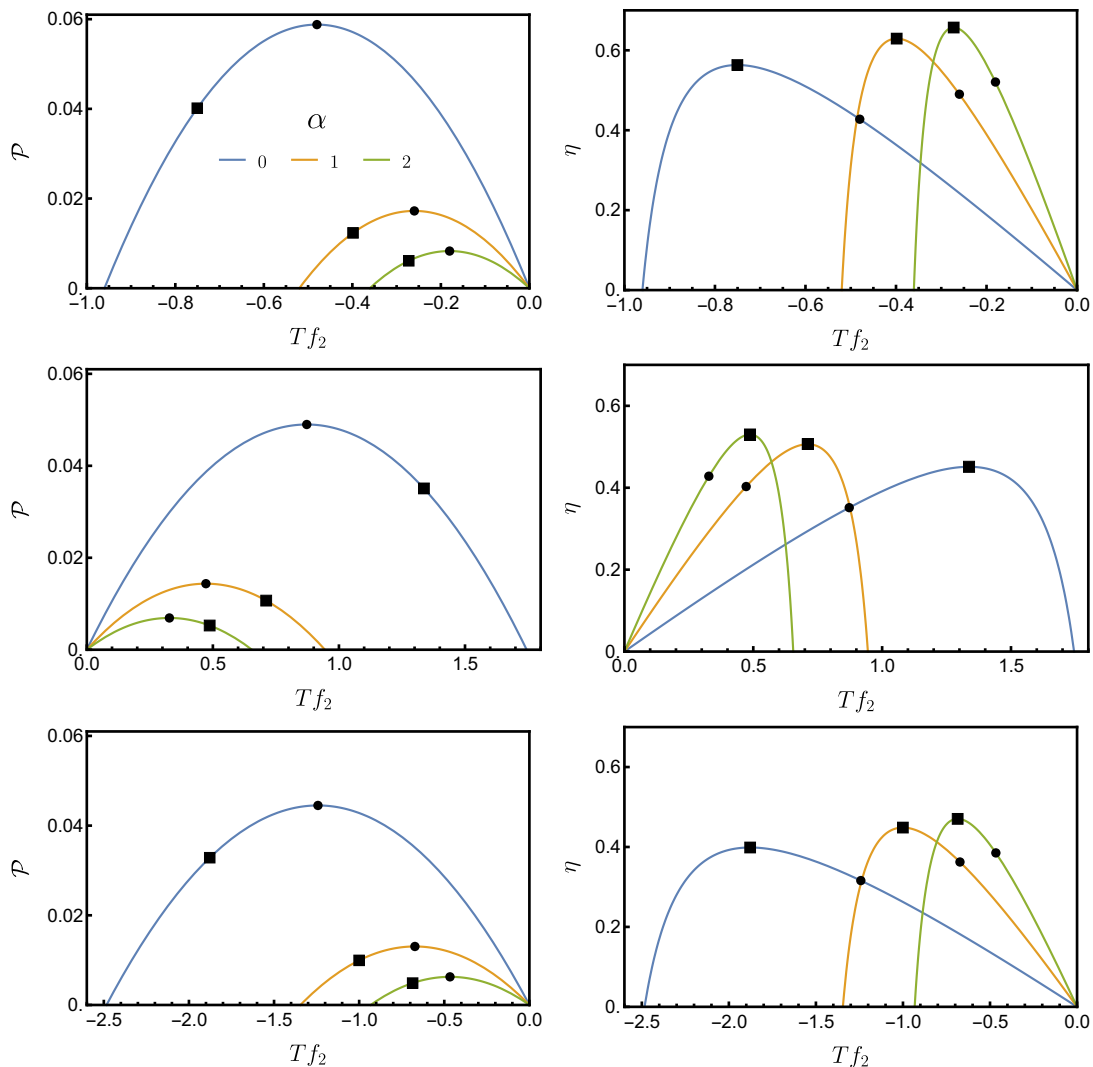


FIG. 4. For power-law drivings, the depiction of power output \mathcal{P} and efficiency η versus $X_2 = Tf_2$ for representative values of α and β (from top to bottom, $\beta = 0, 1$ and 2). Squares and circles denote the maximum efficiencies and powers, according to Eq. (31)-(30). In all cases, we set $X_1 = Tf_1 = 1$, $\tau = \gamma = k_B = m = 1$ and $T = 1/2$.

IV. CONCLUSIONS

The influence of the driving in a collisional approach for Brownian engine, in which the particle is subjected each half stage to a distinct force and driving, was investigated from the framework of stochastic Thermodynamics. General and exact expressions for thermodynamic quantities, such as output power and efficiency were obtained, irrespective the kind of driving, period and temperatures. Distinct routes for the maximization of power and efficiency were undertaken, whether with respect to the strength force, driving and both of them for two kind of drivings: generic power-law and periodically drivings. The engine performance can be strongly affected when one considers simple (and different) power law drivings acting over the system at each stage. While a constant driving is always more advantageous for enhancing the power output, a convenient compromise between force $|f_2|$, α and β can be

adopted for improving the efficiency. Conversely, periodically drivings not only allows to perform a simultaneous maximization of engine, in order to obtain a larger gain, but also the change of driving (exemplified by a phase difference in the second stage) confers a second advantage, in which the engine regime is (substantially) enlarged the engine regime over distinct sets of parameters.

As a final comment, it is worth pointing out the decreasing of engine performance as the difference of temperatures between thermal baths is increased. The inclusion of new ingredients, such as a coupling between velocity and drivings, may be a candidate in order to circumvent this fact and be responsible for a better performance of such class of collisional thermal engines.

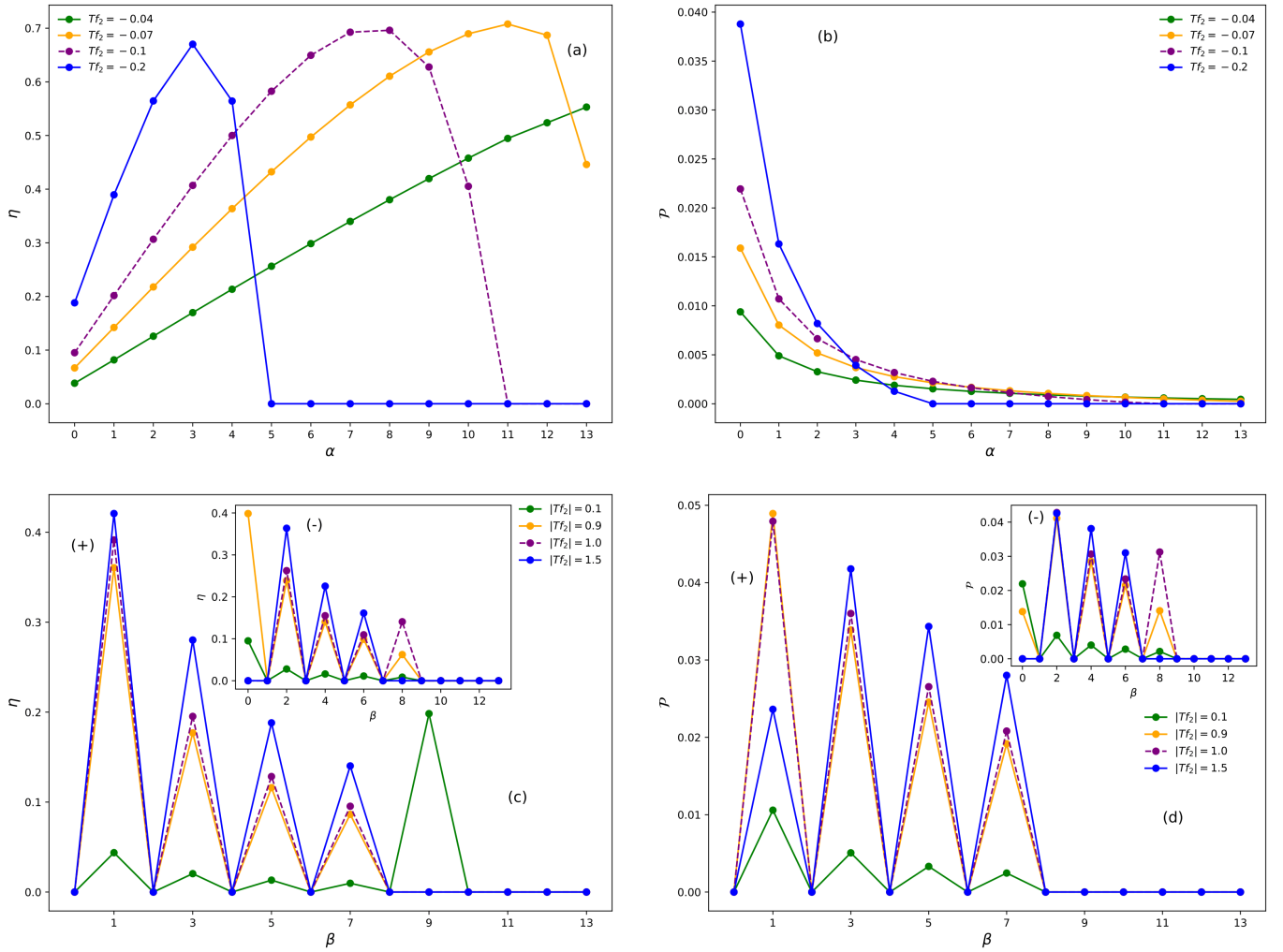


FIG. 5. For fixed forces $X_2 = Tf_2$, the depiction of efficiency η (a) and \mathcal{P} (c) versus α ($\beta = 0$). Panels (b) and (d) show the same, but β is varied (for fixed $\alpha = 0$). Main panels (insets) in (c) and (d) show results for odd (even) β . In all cases, we set $X_1 = Tf_1 = 1$, $\tau = \gamma = k_B = m = 1$ and $T = 1/2$.

V. ACKNOWLEDGMENTS

C.E.F. acknowledges the financial support from São Paulo Research Foundation (FAPESP) under Grants No. 2021/05503-7 and 2021/03372-2. The financial support from CNPq is also acknowledged. This study was supported by the Special Research Fund (BOF) of Hasselt University under grant BOF20BL17.

Appendix A: Onsager coefficients for generic periodically driving

Onsager coefficients for a generic periodic driving in each half stage are listed below:

$$\begin{aligned}
 L_{11} = & \frac{mT}{\tau(e^{\gamma\tau} - 1)} \sum_{n=0}^{\infty} \sum_{m=0}^{\infty} \left\{ (e^{\gamma\tau} - 1) \int_0^{\tau/2} [a_m^{(1)} \cos\left(\frac{4\pi m}{\tau} t\right) + b_m^{(1)} \sin\left(\frac{4\pi m}{\tau} t\right)] [a_n^{(1)} C_n^{(1)}(t) + b_n^{(1)} S_n^{(1)}(t)] e^{-\gamma t} dt + \right. \\
 & \left. + [a_n^{(1)} C_n^{(1)}(\tau/2) + b_n^{(1)} S_n^{(1)}(\tau/2)] [a_m^{(1)} \bar{C}_m^{(1)}(\tau/2) + b_m^{(1)} \bar{S}_m^{(1)}(\tau/2)], \right\} \quad (\text{A1})
 \end{aligned}$$

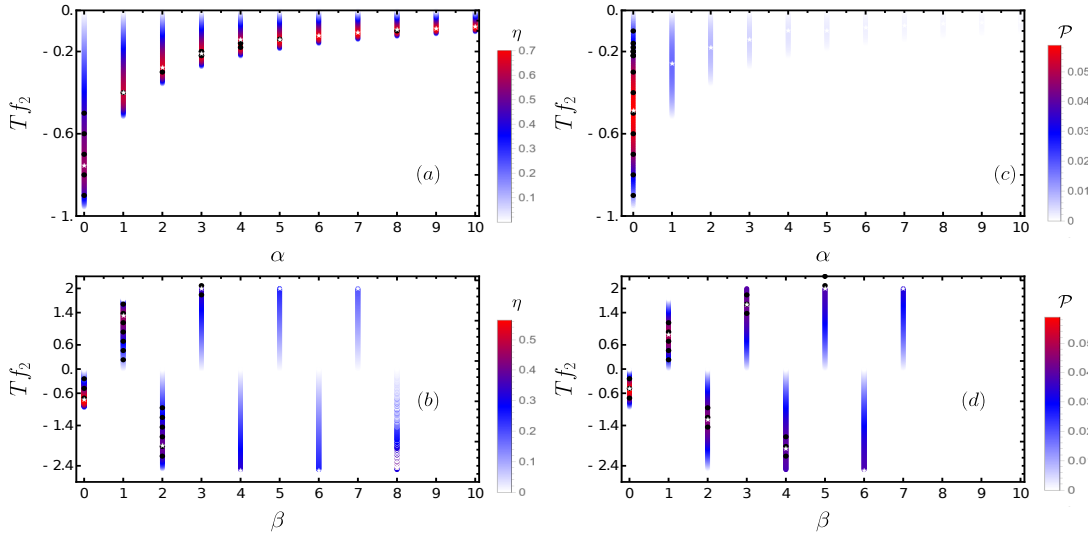


FIG. 6. Panels (a) and (c) depict, for $\beta = 0$, the phase diagram $X_2 = Tf_2$ versus α by considering the efficiency (a) and power (c). In (b) and (d), the opposite case (β is varied for fixed $\alpha = 0$). White and black symbols denote some representative maximizations with respect to the f_2 and driving (for f_2 held fixed), respectively. In all cases, we set $X_1 = Tf_1 = 1$, $\tau = \gamma = k_B = m = 1$ and $T = 1/2$.

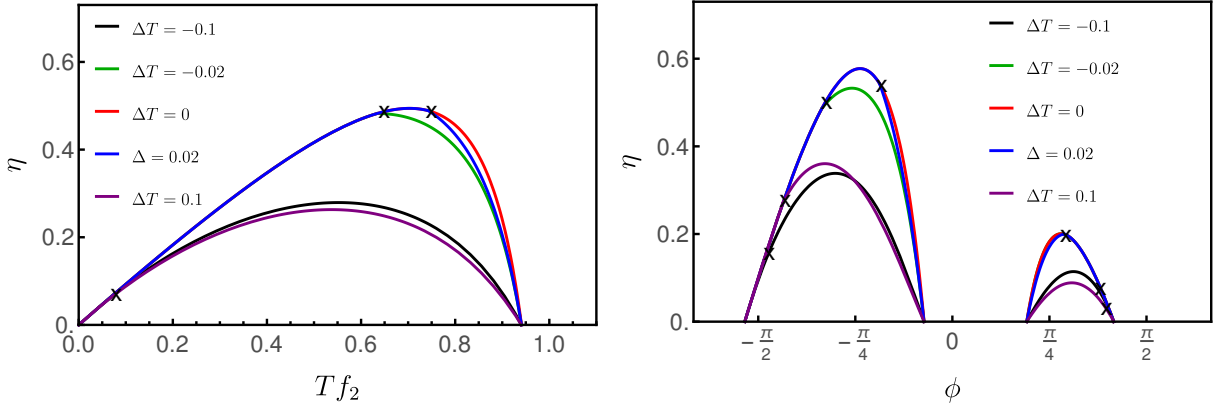


FIG. 7. For $\tau = 2$, $\phi = 0$ and $Tf_2 = 1$, the depiction of efficiency η versus Tf_2 and ϕ for distinct temperature difference ΔT between thermal baths, respectively. Symbols \times attempt to the separatrix between the work-to-work and thermal engines, respectively. In all cases, we set $T_1 = 1/2$, $T_2 = 1/2 + \Delta T$, $X_1 = Tf_1 = 1$ and $\gamma = k_B = m = 1$.

$$L_{22} = \frac{mT}{\tau(e^{\gamma\tau} - 1)} \sum_{n=0}^{\infty} \sum_{m=0}^{\infty} \left\{ (e^{\gamma\tau} - 1) \int_{\tau/2}^{\tau} \left[a_m^{(2)} \cos\left(\frac{4\pi m}{\tau} t\right) + b_m^{(2)} \sin\left(\frac{4\pi m}{\tau} t\right) \right] \{ a_n^{(2)} [C_n^{(1)}(t) - C_n^{(1)}(\tau/2)] + b_n^{(2)} [S_n^{(1)}(t) - S_n^{(1)}(\tau/2)] \} e^{-\gamma t} dt \right. \\ \left. + \{ a_n^{(2)} [C_n^{(1)}(\tau) - C_n^{(1)}(\tau/2)] + b_n^{(2)} [S_n^{(1)}(\tau) - S_n^{(1)}(\tau/2)] \} \{ a_m^{(2)} [\bar{C}_m^{(1)}(\tau) - \bar{C}_m^{(1)}(\tau/2)] + b_m^{(2)} [\bar{S}_m^{(1)}(\tau) - \bar{S}_m^{(1)}(\tau/2)] \} \right\} \quad (\text{A2})$$

$$L_{12} = \frac{mT}{\tau(e^{\gamma\tau} - 1)} \sum_{n=0}^{\infty} \sum_{m=0}^{\infty} \{ a_n^{(2)} [C_n^{(1)}(\tau) - C_n^{(1)}(\tau/2)] + b_n^{(2)} [S_n^{(1)}(\tau) - S_n^{(1)}(\tau/2)] \} \{ a_m^{(1)} \bar{C}_m^{(1)}(\tau/2) + b_m^{(1)} \bar{S}_m^{(1)}(\tau/2) \} \quad (\text{A3})$$

$$L_{21} = \frac{mT e^{\gamma\tau}}{\tau(e^{\gamma\tau} - 1)} \sum_{n=0}^{\infty} \sum_{m=0}^{\infty} \{ a_n^{(1)} C_n^{(1)}(\tau/2) + b_n^{(1)} S_n^{(1)}(\tau/2) \} \{ a_m^{(2)} [\bar{C}_m^{(1)}(\tau) - \bar{C}_m^{(1)}(\tau/2)] + b_m^{(2)} [\bar{S}_m^{(1)}(\tau) - \bar{S}_m^{(1)}(\tau/2)] \}, \quad (\text{A4})$$

where we introduce the following shorthand notation in-

volving quantities $\bar{C}_m^{(i)}(t)$, $C_m^{(i)}(t)$, $\bar{S}_m^{(i)}(t)$ and $S_m^{(i)}(t)$

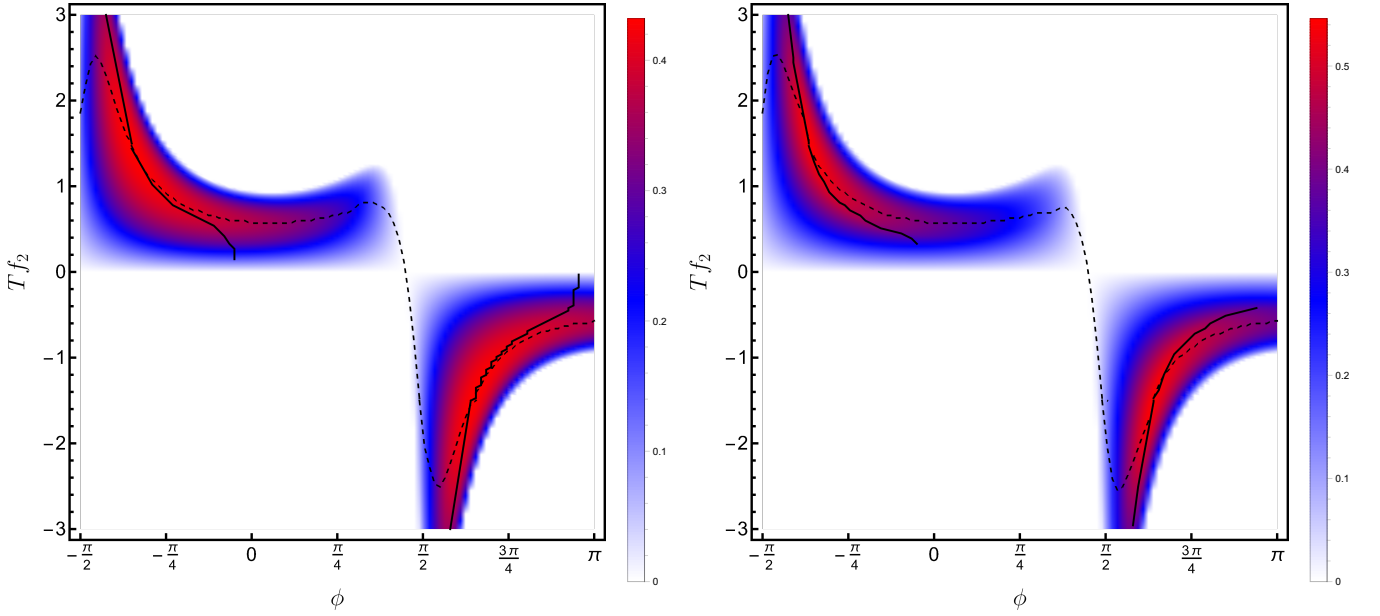


FIG. 8. For the set of drivings given by Eq. (44) and $\tau = 2$, left and right panels depict efficiency phase diagrams of the output force $X_2 = Tf_2$ versus the phase difference ϕ for $\Delta T = 0.1$ and -0.1 , respectively. Continuous and dashed lines denote the maximization with respect to f_2 and ϕ , respectively. In all cases, we set $X_1 = Tf_1 = 1$, $\gamma = k_B = m = 1$ and $T = 1/2$.

$$C_n^{(1)}(t) = \int_0^t e^{\gamma t'} \cos\left(\frac{4\pi n}{\tau} t'\right) dt' \quad (\text{A5})$$

$$\bar{C}_n^{(1)}(t) = \int_0^t e^{-\gamma t'} \cos\left(\frac{4\pi n}{\tau} t'\right) dt' \quad (\text{A6})$$

$$S_n^{(1)}(t) = \int_0^t e^{\gamma t'} \sin\left(\frac{4\pi n}{\tau} t'\right) dt' \quad (\text{A7})$$

$$\bar{S}_n^{(1)}(t) = \int_0^t e^{-\gamma t'} \sin\left(\frac{4\pi n}{\tau} t'\right) dt' \quad (\text{A8})$$

$$(\text{A9})$$

For the particular set of drivings from Eq. (44), and considering $\omega_j = 2\pi/\tau$, Onsager coefficients reduce to the following expressions:

$$L_{11} = \frac{mT\tau \left[\gamma^3 \tau^3 + 4\pi^2 \gamma \tau + 16\pi^2 \coth\left(\frac{\gamma\tau}{4}\right) \right]}{4(\gamma^2 \tau^2 + 4\pi^2)^2}, \quad (\text{A10})$$

$$L_{22} = \frac{mT\tau \left[\gamma \tau \left(\left(e^{\frac{\gamma\tau}{2}} - 1 \right) (\gamma^2 \tau^2 + 4\pi^2) - 4\gamma \tau \left(e^{\frac{\gamma\tau}{2}} + 1 \right) \sin^2(\phi) + 16\pi^2 \left(e^{\frac{\gamma\tau}{2}} + 1 \right) \cos^2(\phi) \right] \right]}{4 \left(e^{\frac{\gamma\tau}{2}} - 1 \right) (\gamma^2 \tau^2 + 4\pi^2)^2}, \quad (\text{A11})$$

$$L_{12} = -\frac{2\pi m T \tau \coth\left(\frac{\gamma\tau}{4}\right) (\gamma \tau \sin(\phi) + 2\pi \cos(\phi))}{(\gamma^2 \tau^2 + 4\pi^2)^2}, \quad (\text{A12})$$

and

$$L_{21} = \frac{2\pi m T \tau \coth\left(\frac{\gamma\tau}{4}\right) (\gamma \tau \sin(\phi) - 2\pi \cos(\phi))}{(\gamma^2 \tau^2 + 4\pi^2)^2}, \quad (\text{A13})$$

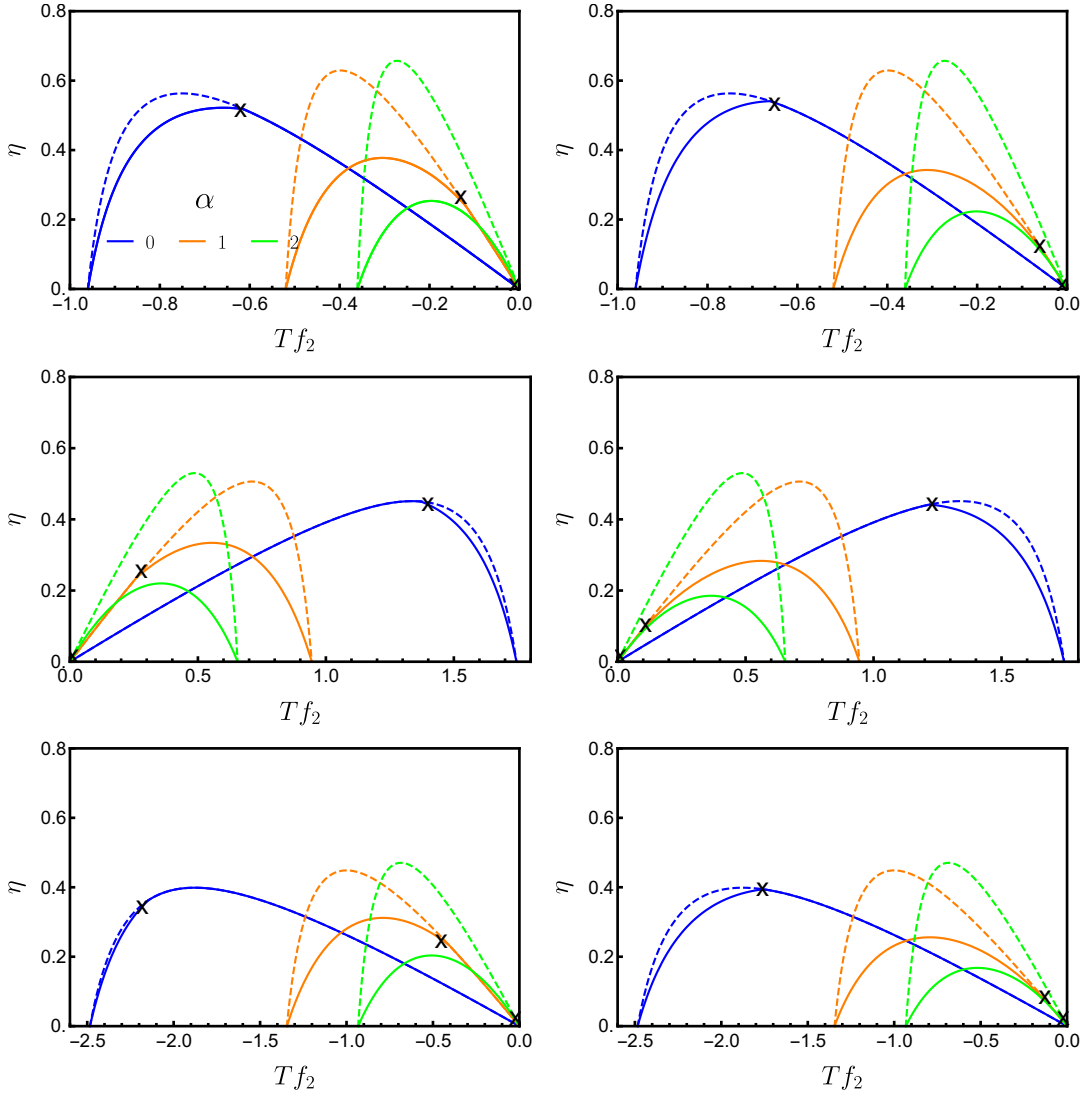


FIG. 9. Left and right panels show the efficiency η versus Tf_2 for distinct α 's for $\Delta T = 0.025$ and $\Delta T = -0.025$, respectively. Symbols \times denote the separatrix between the work-to-work converter (dashed lines) from the heat engine (continuous lines). From top to bottom, $\beta = 0, 1$ and 2 .

respectively.

Appendix B: Onsager coefficients for power-law drivings

For generic algebraic (power-law) drivings, Onsager coefficients are listed below:

$$L_{11} = \frac{mT}{\tau} \int_0^{\tau/2} \left[4^\alpha e^{-t} \left(\frac{t}{\tau} \right)^\alpha \left(\frac{(-\tau)^{-\alpha} \left(\Gamma(\alpha + 1, -\frac{t}{\tau}) - \Gamma(\alpha + 1) \right)}{e^\tau - 1} + (-t)^{-\alpha} \left(\frac{t}{\tau} \right)^\alpha \left(\Gamma(\alpha + 1, -t) - \alpha \Gamma(\alpha) \right) \right) \right] dt, \quad (\text{B1})$$

$$L_{12} = \frac{mT}{\tau} \int_0^{\tau/2} \left[(-1)^\beta e^{-t} 2^{\alpha+\beta-1} (-\tau)^{-\beta} \text{csch} \left(\frac{\tau}{2} \right) \left(\frac{t}{\tau} \right)^\alpha \left(\Gamma(\beta + 1, -\frac{t}{\tau}) - \Gamma(\beta + 1) \right) \right] dt, \quad (\text{B2})$$

$$L_{21} = \frac{mT}{\tau} \int_{\tau/2}^{\tau} \left[\frac{2^\alpha (-\tau)^{-\alpha} e^{\tau-t} \left(1 - \frac{2t}{\tau} \right)^\beta \left(\Gamma(\alpha + 1, -\frac{t}{\tau}) - \Gamma(\alpha + 1) \right)}{e^\tau - 1} \right] dt, \quad (\text{B3})$$

and

$$L_{22} = -\frac{m\Gamma}{\tau(e^\tau - 1)} \int_{\tau/2}^{\tau} \left\{ e^{\frac{\tau}{2}-t} \left(1 - \frac{2t}{\tau} \right)^\beta \left[\left(\frac{2}{\tau} \right)^\beta \left(\Gamma(\beta + 1) - \Gamma\left(\beta + 1, -\frac{\tau}{2}\right) \right) + (e^\tau - 1) \left(2 - \frac{4t}{\tau} \right)^\beta (\tau - 2t)^{-\beta} \left(\Gamma(\beta + 1) - \Gamma\left(\beta + 1, \frac{\tau}{2} - t\right) \right) \right] \right\} dt, \quad (\text{B4})$$

respectively, where $\Gamma(x)$ and $\Gamma(x, y)$ denote gamma and incom-

plete gamma functions, respectively.

-
- [1] M. Esposito, R. Kawai, K. Lindenberg, and C. Van den Broeck, *Phys. Rev. E* **81**, 041106 (2010).
- [2] S. Rana, P. Pal, A. Saha, and A. Jayannavar, *Physical review E* **90**, 042146 (2014).
- [3] I. A. Martínez, É. Roldán, L. Dinis, D. Petrov, J. M. Parrondo, and R. A. Rica, *Nature physics* **12**, 67 (2016).
- [4] J. A. Albay, Z.-Y. Zhou, C.-H. Chang, and Y. Jun, *Scientific reports* **11**, 1 (2021).
- [5] N. Golubeva and A. Imparato, *Phys. Rev. Lett.* **109**, 190602 (2012).
- [6] I. N. Mamede, P. E. Harunari, B. A. N. Akasaki, K. Proesmans, and C. E. Fiore, *Phys. Rev. E* **105**, 024106 (2022).
- [7] Y. Jun, M. Gavrilov, and J. Bechhoefer, *Physical review letters* **113**, 190601 (2014).
- [8] S. De Groot and P. Mazur, “North-holland,” (1962).
- [9] U. Seifert, *Reports on progress in physics* **75**, 126001 (2012).
- [10] C. Van den Broeck, *Physical Review Letters* **95**, 190602 (2005).
- [11] C. Van den Broeck and M. Esposito, *Phys. Rev. E* **82**, 011144 (2010).
- [12] L. Peliti and S. Pigolotti, *Stochastic Thermodynamics: An Introduction* (Princeton University Press, 2021).
- [13] A. Rosas, C. Van den Broeck, and K. Lindenberg, *Phys. Rev. E* **96**, 052135 (2017).
- [14] A. Rosas, C. Van den Broeck, and K. Lindenberg, *Phys. Rev. E* **97**, 062103 (2018).
- [15] C. F. Noa, W. G. Oropesa, and C. Fiore, *Physical Review Research* **2**, 043016 (2020).
- [16] C. E. F. Noa, A. L. L. Stable, W. G. C. Oropesa, A. Rosas, and C. E. Fiore, *Phys. Rev. Research* **3**, 043152 (2021).
- [17] P. E. Harunari, F. S. Filho, C. E. Fiore, and A. Rosas, *Phys. Rev. Research* **3**, 023194 (2021).
- [18] C. H. Bennett, *International Journal of Theoretical Physics* **21**, 905 (1982).
- [19] K. Maruyama, F. Nori, and V. Vedral, *Reviews of Modern Physics* **81**, 1 (2009).
- [20] T. Sagawa, *Journal of Statistical Mechanics: Theory and Experiment* **2014**, P03025 (2014).
- [21] J. M. Parrondo, J. M. Horowitz, and T. Sagawa, *Nature physics* **11**, 131 (2015).
- [22] G. Verley, M. Esposito, T. Willaert, and C. Van den Broeck, *Nature Communications* **5**, 4721 (2014).
- [23] T. Schmiedl and U. Seifert, *EPL (Europhysics Letters)* **81**, 20003 (2007).
- [24] M. Esposito, K. Lindenberg, and C. Van den Broeck, *Physical Review Letters* **102**, 130602 (2009).
- [25] B. Cleuren, B. Ruten, and C. Van den Broeck, *The European Physical Journal Special Topics* **224**, 879 (2015).
- [26] M. Esposito, R. Kawai, K. Lindenberg, and C. Van den Broeck, *Physical Review E* **81**, 041106 (2010).
- [27] U. Seifert, *Physical Review Letters* **106**, 020601 (2011).
- [28] Y. Izumida and K. Okuda, *Europhysics Letters* **97**, 10004 (2012).
- [29] N. Golubeva and A. Imparato, *Physical Review Letters* **109**, 190602 (2012).
- [30] V. Holubec, *Journal of Statistical Mechanics: Theory and Experiment* **2014**, P05022 (2014).
- [31] M. Bauer, K. Brandner, and U. Seifert, *Physical Review E* **93**, 042112 (2016).
- [32] K. Proesmans, C. Driesen, B. Cleuren, and C. Van den Broeck, *Physical review E* **92**, 032105 (2015).
- [33] K. Proesmans, Y. Dreher, M. Gavrilov, J. Bechhoefer, and C. Van den Broeck, *Physical Review X* **6**, 041010 (2016).
- [34] V. Holubec and A. Ryabov, *Phys. Rev. E* **92**, 052125 (2015).
- [35] R. S. Johal, *Phys. Rev. E* **100**, 052101 (2019).
- [36] A. Purkayastha, G. Guarnieri, S. Campbell, J. Prior, and J. Gould, *arXiv preprint arXiv:2202.05264* (2022).
- [37] P. H. Jones, O. M. Maragò, and G. Volpe, *Optical tweezers: Principles and applications* (Cambridge University Press, 2015).
- [38] J. A. Albay, G. Paneru, H. K. Pak, and Y. Jun, *Optics express* **26**, 29906 (2018).
- [39] A. Kumar and J. Bechhoefer, *Applied Physics Letters* **113**, 183702 (2018).
- [40] G. Paneru and H. Kyu Pak, *Advances in Physics: X* **5**, 1823880 (2020).
- [41] J. Li, J. M. Horowitz, T. R. Gingrich, and N. Fakhri, *Nature communications* **10**, 1 (2019).
- [42] S. Krishnamurthy, S. Ghosh, D. Chatterji, R. Ganapathy, and A. Sood, *Nature Physics* **12**, 1134 (2016).
- [43] V. Blickle and C. Bechinger, *Nature Physics* **8**, 143 (2012).
- [44] P. A. Quinto-Su, *Nature communications* **5**, 1 (2014).
- [45] A. C. Barato and U. Seifert, *Phys. Rev. X* **6**, 041053 (2016).
- [46] K. Proesmans and J. M. Horowitz, *Journal of Statistical Mechanics: Theory and Experiment* **2019**, 054005 (2019).
- [47] V. Holubec and A. Ryabov, *Phys. Rev. Lett.* **121**, 120601 (2018).
- [48] T. Tomé and M. J. De Oliveira, *Stochastic dynamics and irreversibility* (Springer, 2015).
- [49] T. Tomé and M. J. de Oliveira, *Physical Review E* **82**, 021120 (2010).
- [50] S. Liepelt and R. Lipowsky, *Phys. Rev. Lett.* **98**, 258102 (2007).
- [51] S. Liepelt and R. Lipowsky, *Phys. Rev. E* **79**, 011917 (2009).
- [52] H. Hooijberghs, B. Cleuren, A. Salazar, J. O. Indekeu, and C. Van den Broeck, *J. Chem. Phys.* **139**, 134111 (2013).
- [53] K. Proesmans and C. Van den Broeck, *Chaos: An Interdisciplinary Journal of Nonlinear Science* **27**, 104601 (2017).
- [54] B. A. Akasaki, M. J. de Oliveira, and C. E. Fiore, *Physical Review E* **101**, 012132 (2020).